

Lead-Free Polycrystalline Ferroelectric Nanowires with Enhanced Curie Temperature

Anuja Datta, Pedro E. Sanchez-Jimenez, Rabih Al Rahal Al Orabi, Yonatan Calahorra, Canlin Ou, Suman-Lata Sahonta, Marco Fornari, and Sohini Kar-Narayan*

Ferroelectrics are important technological materials with wide-ranging applications in electronics, communication, health, and energy. While lead-based ferroelectrics have remained the predominant mainstay of industry for decades, environmentally friendly lead-free alternatives are limited due to relatively low Curie temperatures (T_C) and/or high cost in many cases. Efforts have been made to enhance T_C through strain engineering, often involving energy-intensive and expensive fabrication of thin epitaxial films on lattice-mismatched substrates. Here, a relatively simple and scalable sol-gel synthesis route to fabricate polycrystalline $(\text{Ba}_{0.85}\text{Ca}_{0.15})(\text{Zr}_{0.1}\text{Ti}_{0.9})\text{O}_3$ nanowires within porous templates is presented, with an observed enhancement of T_C up to $\approx 300^\circ\text{C}$ as compared to $\approx 90^\circ\text{C}$ in the bulk. By combining experiments and theoretical calculations, this effect is attributed to the volume reduction in the template-grown nanowires that modifies the balance between different structural instabilities. The results offer a cost-effective solution-based approach for strain-tuning in a promising lead-free ferroelectric system, thus widening their current applicability.

attracted considerable attention,^[2,3] due to confinement-induced enhancement of polarization and strain-mediated depolarizing effect in nanodomains that give rise to improved ferroelectric as well as piezoelectric properties.^[4,5] For example, it has been theoretically predicted,^[4,6–10] and experimentally reported,^[2,3,11–17] that strain engineering in ferroelectric epitaxial films on lattice mismatched substrates can facilitate large shifts in the Curie temperature (T_C) and enhancement in the remanent polarization (P_r) of these materials. These effects are especially useful in the case of lead-free ferroelectrics with low T_C which often limits their practical use. However, the use of substrate-induced epitaxial strain is limited to thin films with thicknesses of the order of tens of nanometers, beyond which strain relaxation occurs.^[14] Recent studies have shown that nanostructuring could

1. Introduction

Ferroelectric materials have been widely investigated for decades as the building blocks for applications ranging from transducers and energy harvesters to nonvolatile memory and transistor devices.^[1] In particular, low-dimensional ferroelectrics have

provide a new route to strain engineering in ferroelectrics,^[14] where size-effect plays a dominant role in determining not only the ferroelectric polarization but also the piezoelectric responses from these materials. Induced strain due to dimensional confinement in nanowires (NWs) modifies the ferroelectric properties, such as the T_C , permittivity or polarizability, thereby eventually extending the operational temperature range and overall performance of the devices. As ferroelectricity and piezoelectricity arise from cooperative effects of crystal dimensions, orientation, and ordering, scalable synthesis methodologies that can lead to the manipulation of size and dimensions of ferroelectric nanostructures can offer great advantages.

With respect to lead-free ferroelectrics, studies concerning strain-induced variation of ferroelectric properties in 1D nano-materials are rare.^[2,16,18] Amongst lead (Pb)-free ferroelectrics in the bulk, $x\text{Ba}(\text{Ti}_{0.8}\text{Zr}_{0.3})\text{O}_3 \cdot (1-x)(\text{Ba}_{0.7}\text{Ca}_{0.3})\text{TiO}_3$ where $x = 0.5$,^[19] otherwise known as $(\text{Ba}_{0.85}\text{Ca}_{0.15})(\text{Zr}_{0.1}\text{Ti}_{0.9})\text{O}_3$, or BCT-0.5BZT, is particularly promising as it has soft ferroelectric properties at room temperature (remanent polarization $P_r \approx 10\text{--}15 \mu\text{C cm}^{-2}$, and coercive field $E_C \approx 1.5\text{--}3 \text{ kV cm}^{-1}$) in combination with a large piezoelectric coefficient ($\approx 620 \text{ pC N}^{-1}$), that is comparable to Pb-based $\text{Pb}_x\text{Zr}_{1-x}\text{TiO}_3$ (PZT),^[19] as well as Pb-free $(\text{K},\text{Na})\text{NbO}_3$.^[20] Liu and Ren^[19] reported the phase diagram of the BCT-BZT system, in which they showed a “tilted morphotropic phase boundary” (MPB) separating rhombohedral (R) and tetragonal (T) phases. The presence of a tricritical point between cubic (C)–R–T phases was reported as similar to that found in Pb-based materials.^[21,22] It was pointed out that along

Dr. A. Datta, Dr. Y. Calahorra, C. Ou, Dr. S.-L. Sahonta, Dr. S. Kar-Narayan
Department of Materials Science & Metallurgy
University of Cambridge
27 Charles Babbage Road, Cambridge CB3 0FS, UK
E-mail: sk568@cam.ac.uk

Dr. P. E. Sanchez-Jimenez
Instituto de Ciencia de Materiales de Sevilla
C.S.I.C.-Universidad de Sevilla
C. Américo Vespucio n° 49, 41092 Sevilla, Spain

Dr. R. A. R. Al Orabi,^[†] Prof. M. Fornari
Department of Physics and Science of Advanced Materials Program
Central Michigan University
Mt. Pleasant, MI 48859, USA

© 2017 The Authors. Published by WILEY-VCH Verlag GmbH & Co. KGaA, Weinheim. This is an open access article under the terms of the Creative Commons Attribution License, which permits use, distribution and reproduction in any medium, provided the original work is properly cited.

^[†]Present address: Design and Development of Functional Materials Department, AXEL'ONE Collaborative Platform - Innovative Materials, 87 rue des freres Perret - BP62 69192 Saint FONS Cedex, France

The ORCID identification number(s) for the author(s) of this article can be found under <https://doi.org/10.1002/adfm.201701169>.

DOI: 10.1002/adfm.201701169

this MPB, the polarization has enhanced response to external stress and/or electric fields due to phase transition instabilities within a narrow temperature range resulting from the low energy barriers between different polar distortions, allowing for easy rotation of the polarization direction.^[19,23–25] More specifically the properties can be justified in terms of the interplay between the off-centerings of Ti, Zr (mostly in the rhombohedral direction), and of Ca (mostly in the tetragonal direction) with chemical disorder (Section S1 and Figure S1, Supporting Information). Regardless of the near room-temperature MPB of BCT-0.5BZT, the bulk material exhibits a T_C of about 90 °C and a large temperature dependence of the properties,^[19] which limit application in practical devices. In order to improve the T_C , we adopt, in this work, a nanoconfinement-based approach to tune the strain and the ferroelectric properties in NWs of this material.

Here we report a novel and facile synthesis of highly crystalline BCT-0.5BZT NWs fabricated using a sol–gel assisted template-wetting methodology. This approach is cost-effective and largely scalable expanding its viability to other Pb-free ferroelectric materials systems at the nanoscale. Our combined sol–gel and template-assisted fabrication route results in well-controlled uniform growth of high aspect ratio, highly crystalline BCT-0.5BZT nanowires, as compared to more complex multi-step hydrothermal synthesis,^[26] or electrospinning.^[27] The structural, ferroelectric and dielectric properties of BCT-0.5BZT NW arrays were successfully measured for as-prepared template-freed nanowires and studied in terms of the effects of reduced dimensionality and strain due to lattice distortion as well as grain boundaries. Overall the measured T_C was found to greatly increase with respect to the bulk value, reaching ≈ 300 °C. Additionally, the piezoelectric coupling coefficient measured by piezoresponse force microscopy (PFM) indicates BCT-0.5BZT NWs to be a promising alternative to Pb-based piezoceramics. Our experimental findings are interpreted with the aid of first-principles calculations that clarify the consequences of our novel template-assisted synthesis method. In particular, the calculations highlight the effect of strain on the structure and, indirectly, on T_C .

2. Results and Discussion

2.1. Growth and Morphology of BCT-0.5BZT Nanowires

BCT-0.5BZT NWs were prepared through a two-step chemical synthesis process, shown schematically in **Figure 1a** that includes (i) preparation of the BCT-0.5BZT sol and subsequent infiltration of the sol in track-etched polyimide (PI) porous templates of pore diameter ≈ 200 nm and thickness ≈ 20 μm , and (ii) annealing the sol-filled PI template at 1000 °C in air to crystallize the BCT-0.5BZT ceramic phase. The two-step synthesis process aided by vacuum-assisted template pore-confinement ensures phase-pure BCT-0.5BZT NW arrays following the reaction mechanism given in Section S2 of the Supporting Information. The vacuum driving force was found to be highly effective, without which incomplete infiltration resulted that led to disrupted crystallite growth in contrast to long nanowires obtained when assisted with vacuum (Figure S2, Supporting

Information). The high thermal stability^[28] of the PI template allowed for the organic Ba, Ca, Zr, and Ti precursor sol to consolidate within the pores even before the onset of the decomposition of the template, as observed from Fourier transform infrared (FTIR) spectroscopy, X-ray diffraction (XRD), and thermogravimetric and differential thermal analysis (TGA-DTA) (see Section S3 and Figure S3, Supporting Information). The NWs were found to endure the thermal stress generated from the subsequent decomposition of the host PI template, without losing their dimensional integrity. Continuous mass loss was observed from TGA-DTA when heated till 1000 °C, due to the successive loss of structural water, solvents, and the polymeric PI template, leading up to the formation of the BCT-0.5BZT ceramic (Section S3 and Figure S3, Supporting Information). Using this procedure, a dense mat of BCT-0.5BZT NWs was finally obtained as shown in the scanning electron microscope (SEM) image in Figure 1b. The NWs were observed to be dimensionally uniform and closely retained the morphology of the template pores with thickness and length of ≈ 200 nm and ≈ 20 μm , respectively (Figure 1b,c). Figure 1d and its inset show the transmission electron microscope (TEM) images of BCT-0.5BZT NWs where it can be clearly seen that the NWs were of a polycrystalline nature and comprised polygonal crystallites. Irrespective of their polycrystalline nature, the NWs were mechanically stable and retained their lengths after ≈ 1 h of ultra-sonication during TEM sample preparation, as revealed from the TEM image. Figure 1e shows the high-resolution TEM (HRTEM) image of one BCT-0.5BZT crystallite, indicating the lattice fringe spacing of plane (110) = 0.28 nm of phase-pure rhombohedral BaTiO₃. Selected area electron diffraction (SAED) pattern of the BCT-0.5BZT NWs (Figure 1f) indicated a highly crystalline ring pattern with identifiable major diffraction planes of rhombohedral BaTiO₃ and energy-dispersive X-ray spectroscopy (EDX) (Figure S4, Supporting Information) revealed near stoichiometry composition of (Ba_{0.85}Ca_{0.15})(Zr_{0.1}Ti_{0.9})O₃ with 98% average certainty (based on the EDX detector arrangement, plus correction factors of the instrument), as recorded from several NWs.

2.2. Crystal Structure and Phase of BCT-0.5BZT Nanowires

XRD and Raman spectroscopy studies of annealed NWs (**Figure 2**) show pure perovskite phase at room temperature without noticeable impurities within the limits of the instrumental resolution. In order to compare the structure of the bulk BCT-0.5BZT with the NWs, a cylindrical pellet of identical composition was fabricated by solid-state reaction and subsequently characterized (Section S4 and Figure S5, Supporting Information). At room temperature, the bulk sample prepared by solid-state reaction exhibited the expected tetragonal perovskite phase as Rietveld refinement also yielded a pure phase P4mmm symmetry (Figure 2a; Figures S5 and S6 and Table S1, Supporting Information). However, the NWs were found to preferentially adopt a rhombohedral symmetry (inset of Figure 2a) as suggested by the single reflection at $2\theta = 45^\circ$ (Figure 2a). Possible minor presence of other phases, as well as the effect of peak broadening due to small crystallite size, cannot be ruled out in the nanowires, but are below the resolution limits of the

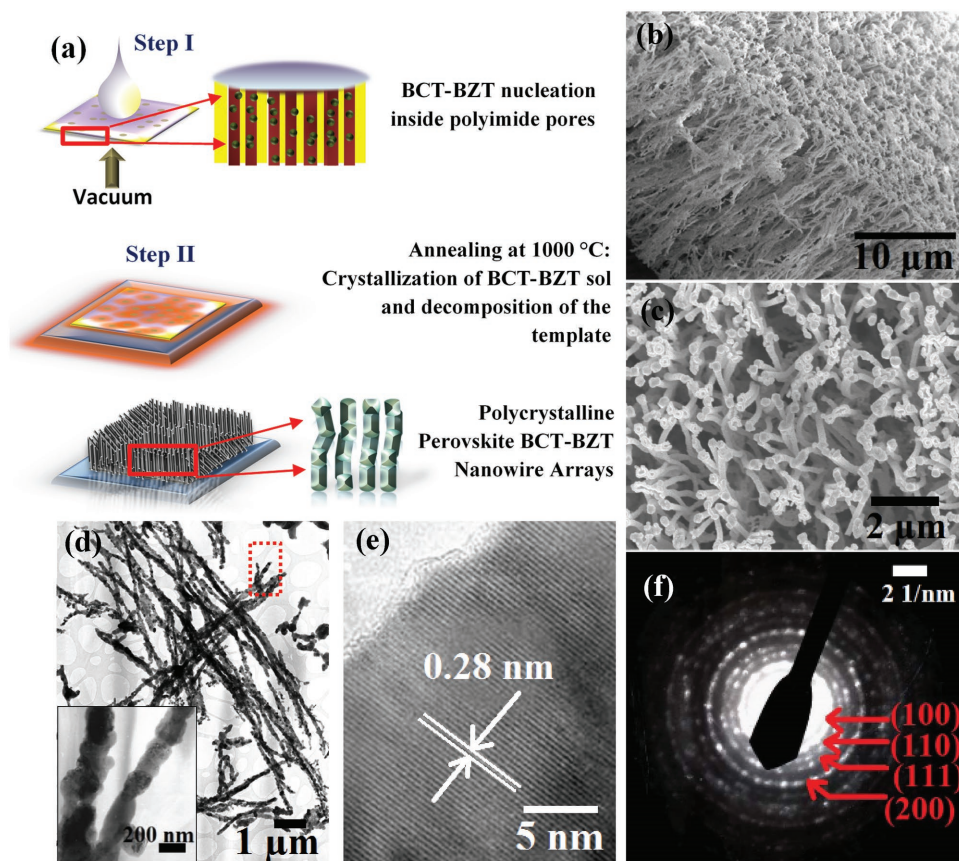


Figure 1. Fabrication and morphology of template-grown lead-free nanowires. a) Schematic illustration of the fabrication steps of $(\text{Ba}_{0.85}\text{Ca}_{0.15})$ $(\text{Zr}_{0.1}\text{Ti}_{0.9})\text{O}_3$ (BCT-0.5BZT) nanowire arrays in porous polyimide template. SEM images, b) side view, and c) top view of the BCT-0.5BZT nanowire arrays obtained after template removal by high temperature annealing. d) TEM image of BCT-0.5BZT nanowires showing polycrystalline crystallites (inset). e) HRTEM image of a BCT-0.5BZT nanowire showing that strongest $d(110) = 0.28$ nm plane spacing. f) Well crystalline SAED pattern of BCT-0.5BZT nanowires indicating the major diffraction planes.

XRD and hence undetectable by Rietveld fitting (Rietveld fitting shown in Figure S6, Supporting Information and Rietveld parameters shown in Table S1, Supporting Information). Similar conclusions were obtained from the Raman spectra, although broadbands appeared due to the polycrystalline nature of the NWs. Introducing Ca and Zr as substituents in A and B positions in the ABO_3 perovskite structure often leads to a compositional disorder that further broadens the Raman bands and shifts their positions. Nevertheless, the small $\text{A}_1(\text{LO})$ band at 189 cm^{-1} served as a convenient signature of the rhombohedral phase, as well as the shift of the 250 cm^{-1} band toward lower frequencies. The $\text{B}_1/\text{E}(\text{TO}_3)$ at 297 cm^{-1} mode indicated the presence of the tetragonal phase which was not observed in the NWs within the resolution limit of the Raman instrument suggesting almost pure phase rhombohedral NWs.^[18,21,23,27,29]

2.3. Ferroelectricity and Piezoelectric Response in BCT-0.5BZT Nanowires

Figure 3a shows the polarization versus electric field (P - E) measurements on a BCT-0.5BZT NW network film. The high yield of our facile and scalable synthesis method enabled us to

prepare large quantities of BCT-0.5BZT NWs for casting into a dense NW network film of $\approx 5\text{ }\mu\text{m}$ in thickness as described in the Experimental Section and as shown in Figure 3b. The dense network structure with long nanowires still preserved (inset of Figure 3b), largely prevented electrical shorting of the sample during the measurement cycles. From the P - E measurements, the BCT-0.5BZT NWs showed clear hysteresis loops till $50\text{ }^\circ\text{C}$, although polarization was found to increase with temperature indicating that at these temperatures, the material is not fully in a pure ferroelectric tetragonal phase, unlike what is expected in the bulk. This is confirmed by dielectric permittivity measurements presented in the next section. At higher temperatures, the adhesion of the NWs with the electrodes became poor due to differential thermal expansion of the NWs and the electrodes and causing difficulty in measuring the P - E loops. While the NW sample showed atypical dielectric nature at room temperature, a strong hysteresis was recorded at $30\text{ }^\circ\text{C}$ with a remanent polarization (P_r) of $3\text{ }\mu\text{C cm}^{-2}$ which increased to $P_r \approx 6\text{ }\mu\text{C cm}^{-2}$ at $50\text{ }^\circ\text{C}$ and a coercive field $E_c \approx 3\text{ kV cm}^{-1}$. The increased area of hysteresis with increasing temperature possibly arose due to increased leakage (Section S5 and Figure S7, Supporting Information) and space-charge effects, as typically observed in other reported ferroelectric NW arrays.^[30–33] Low

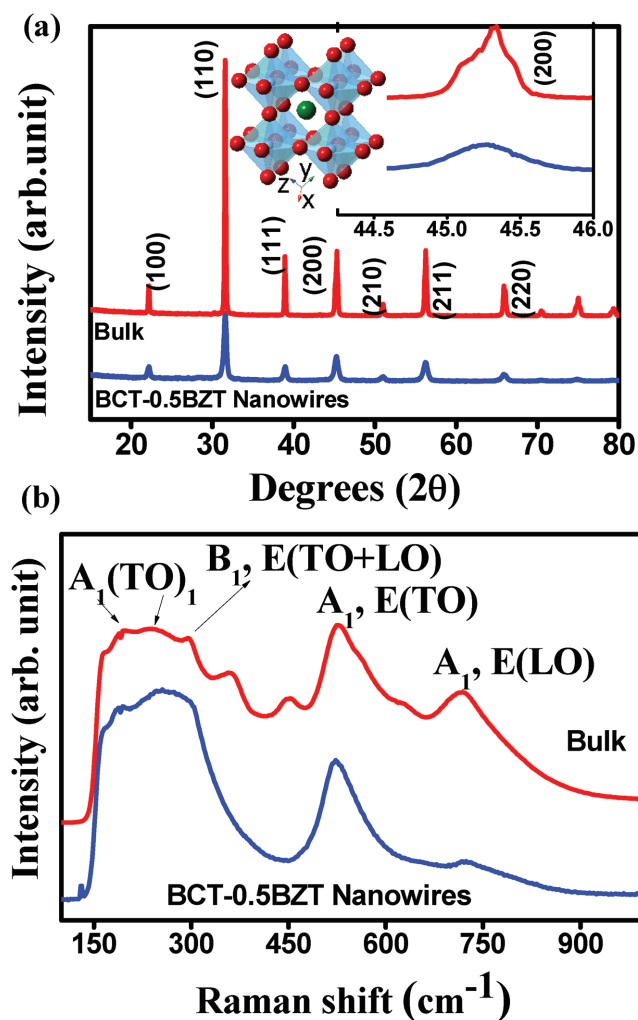


Figure 2. Structural characterization of BCT-0.5BZT nanowires. a) XRD patterns of BCT-0.5BZT nanowire arrays and prepared bulk samples. Inset shows the (200) peak at $2\theta \approx 45^\circ$ indicating the peak broadening in BCT-0.5BZT nanowires as compared to the bulk, likely due to the strain and small crystallite size effect. Also shown in the inset is the rhombohedral crystal structure obtained from Rietveld fitting of the NW XRD. b) Room temperature Raman spectra of BCT-0.5BZT nanowires and bulk.

remnant polarization in nanostructured ferroelectric materials are commonly observed in Pb-free,^[33] and in state-of-the-art PZT nanostructured system^[34] due to their relatively intricate field distribution that are far more complex than in bulk or typical thin film systems. Figure 3c shows an atomic force microscope (AFM) topographic image of the NWs network and hysteresis loops as measured by PFM (Figure 3d) obtained by tapping-mode from the centre of the image (calibration sample results provided in Figure S8, Supporting Information). Figure 3d shows the averaged piezoelectric displacement versus offset voltage and phase versus voltage plots. While the butterfly loops indicated polarization direction reorientation in the BCT-0.5BZT ferroelectric NWs, the observed phase shift clearly demonstrated the local polarization switching behavior in these NWs. The effective piezoelectric coefficient ($d_{33,\text{eff}}$) of the BCT-0.5BZT NW network was estimated using the following

equation and through deflection correlation (the procedure is described in detail elsewhere)^[35,36]

$$d_{33,\text{eff}} = \frac{D - D_0}{V - V_0} \quad (1)$$

Here D_0 and V_0 are, respectively, the displacement and voltage at the intersection of the two sweep-direction graphs (subtracted to eliminate offsets). The result is shown in Figure 3e where a $d_{33,\text{eff}} \approx 35 \text{ pmV}^{-1}$ was obtained. This is slightly lower than a previous report of d_{33} in BCT-0.5BZT NWs,^[26] which could be related to an averaging effect from the unoriented NW network as the domain size has a strong dependence on crystallite size in nanomaterials,^[2,4,5,15,18,29–32] or due to the fact that our NWs are far below T_C at room temperature, unlike their bulk counterpart.

2.4. Enhancement of Curie Temperature in BCT-0.5BZT Nanowires

In order to measure the dielectric properties of BCT-0.5BZT NWs, an NW network structure similar to that prepared for ferroelectric/piezoelectric measurements was used, with Au-coated Si as the bottom electrode and Ag epoxy as the top electrode, as shown in Figure 4a. Preservation of nanowire geometry and simultaneous adhesion to the substrate was achieved for measurements of the BCT-0.5BZT nanowire network, as can be seen from the image. Figure 4b shows the dielectric constant (ϵ_r) as a function of temperature and frequency in the nanowire system, which was compared with the bulk (Figure 4a,b, respectively). Two distinct phase transitions were clearly observed in both the NWs as well as in the bulk sample. While the first transition in the bulk sample (inset I in Figure 4a) was recorded below room temperature ($\approx 18^\circ\text{C}$) the second transition corresponding to a ferroelectric-to-paraelectric transition was recorded at about $T_C \approx 90^\circ\text{C}$, as predicted by the phase diagram of the BCT-0.5BZT composition,^[19] BCT-0.5BZT NWs, however, showed two dielectric anomalies at $\approx 110^\circ\text{C}$ and $\approx 300^\circ\text{C}$, indicating two distinct phase transitions (Figure 4b), with the second one being stronger. These two peak temperatures correspond to rhombohedral–tetragonal (R–T) structural transition (as shown enlarged in inset II), and tetragonal–cubic (T–C) structural transition in BCT-0.5BZT NWs which were enhanced by $\approx 100^\circ\text{C}$ and $>200^\circ\text{C}$, for the R–T and T–C transitions respectively, as compared to the bulk and other similarly reported values in the literature^[19] (see also Figure S9, Supporting Information). The appearance of the first transition confirms that unlike in the bulk, the rhombohedral phase was stabilized in the NWs at room temperature. A peak ϵ_r value of ≈ 6000 was measured at 10 kHz (Figure 4b) from the BCT-0.5BZT NWs (inset II). No shift in these peak positions was observed with frequency, indicating a regular, rather than diffuse, phase transition (Figure 4b).^[37] However, the absolute value of ϵ_r for the T–C transition rapidly decreased with increasing frequency showing the highest value of $\approx 88\,000$ for 1 kHz (Figure S9, Supporting Information). The observed decrease in the dielectric constant with increasing frequency could be due to the dipoles present in the NW network not

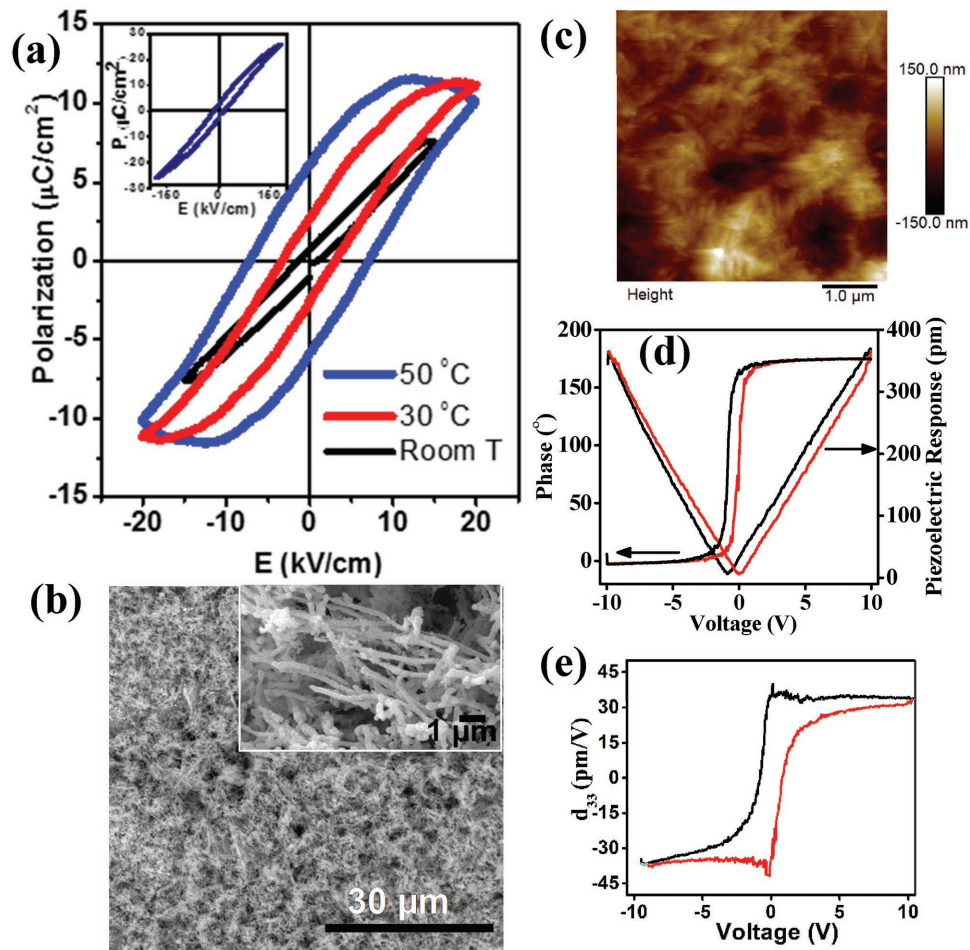


Figure 3. Ferroelectric and piezoelectric characterization a) P - E hysteresis loops from BCT-0.5BZT nanowire network device at room temperature, 30 and 50 °C. P - E hysteresis loop for bulk BCT-0.5BZT taken at room temperature is shown in the inset for comparison. b) An SEM image of the dense BCT-0.5BZT nanowire network. Inset of (b) shows the structure of the BCT-0.5BZT nanowires within the network. c) AFM image of the dense BCT-0.5BZT nanowire network from which the PFM phase shift and d) piezoelectric response have been obtained. e) A d_{33} value of ≈ 35 pmV^{-1} was calculated from the piezoelectric response.

being able to reorient themselves fast enough, thereby exhibit the “quenching” effect, which is commonly observed in ferroelectric nanosystems.^[2,38] The permittivity values of BCT-0.5BZT NWs and that of the bulk above T_C could be linearly fitted maintaining Curie–Weiss law^[39] thus ruling out relaxor behavior in our BCT-0.5BZT NWs (Figure 4c, Supporting Information). The BCT-0.5BZT NWs were also found to have low loss factor in the entire temperature range of measurement, as shown in Figure 4d, values of which were comparable with other nanoferroelectric systems.^[38,40] The observed low dielectric loss in our BCT-BZT NWs indicates that the measured hysteresis loops, as well as the dielectric peak anomaly at 300 °C, are not related to conductivity phenomena.

2.5. Temperature-Dependent XRD Studies and First-Principles Calculations

In order to understand whether the enhancement of T_C observed in our BCT-0.5BZT NWs was inherent, we

performed high-temperature XRD measurements as shown in Figure 5a that indicated a consistent shift of the peak positions to the lower 2θ , likely due to thermal expansion in the NWs. Figure 5b shows the comparison between the lattice parameters (Section S6, Supporting Information) of bulk and NW samples as a function of temperature. At room temperature the unit volume of the NWs was reduced by 2% as compared to the bulk and it remained consistently so. An overall decrease in the lattice parameters ratio, c/a , was revealed for bulk BCT-0.5BZT samples as the temperature increased above the T–C phase transition that was observed at ≈ 90 °C, in agreement with the dielectric permittivity measurements. For BCT-0.5BZT NWs, two sharp changes in the c/a values were observed, which were consistent with the changes in the dielectric permittivity values around the R–T and T–C peak temperatures measured for the NWs. In the tetragonal region, the c/a data were found to fluctuate around an average value of 1.006 that compared reasonably well with the value for the bulk sample below 90 °C. It is important to note that our observation of a rhombohedral phase at room temperature in the NWs was also consistent

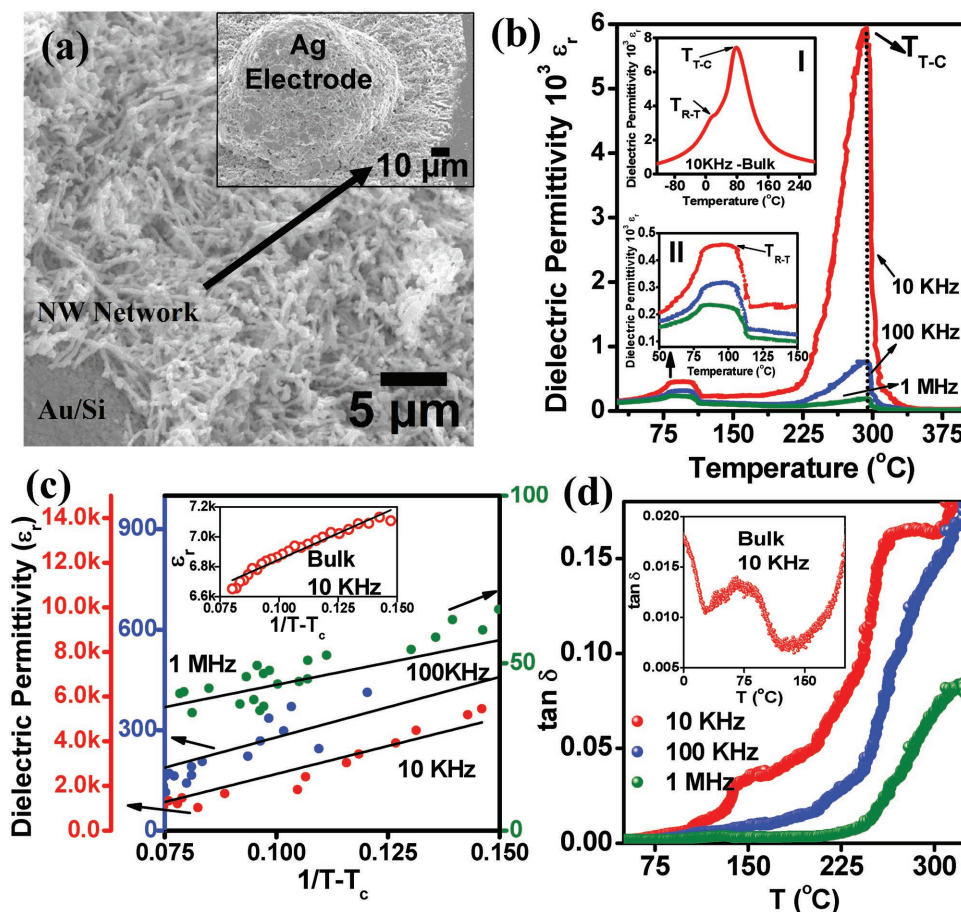


Figure 4. Dielectric characteristics a) SEM image of the BCT-0.5BZT nanowire network on Au/Si showing adherence to the substrate. Inset shows the structure of an Ag electrode used to measure the dielectric properties. b) Dielectric permittivity of BCT-0.5BZT nanowires at different frequencies and that of bulk at 10 KHz, shown as a function of temperature. BCT-0.5BZT nanowires show two clear phase transitions as against only one found in the bulk and around three times enhanced Curie temperature for tetragonal-cubic transition as shown in inset I. An unchanged Curie temperature peak position in the nanowires indicates sharp ferroelectric–paraelectric transition. The R–T transition in nanowires at different frequencies is shown in inset II. c) BCT-0.5BZT nanowires follow Curie–Weiss law as shown for different frequencies. The inset shows that the law similarly follows for BCT-0.5BZT bulk. d) Dielectric loss tangent as shown for BCT-0.5BZT nanowires and bulk (inset).

with the relatively low $d_{33,\text{eff}}$ measured at room-temperature, as compared to reported bulk values in which the phase was purely ferroelectric tetragonal at room temperature.^[2,3,14–16,18,19]

We performed first-principles calculations using a Ba₇CaTi₇ZrO₂₄ supercell that closely approximated the experimental composition (Section S7, Supporting Information). In order to evaluate the effect of strain on the local distortions we performed volume constrained structural relaxations and analyzed the cations' off-centerings and octahedral rotations.^[41,42] In the spirit of the quasi-harmonic approximations, the effect of temperature can be simulated controlling the unit cell volume: we found that Ti ions favor [111] displacements under compression but switch to [001] off-centerings when the volume expands. Ca off-centers in the [111] direction whereas Ba and Zr are largely inactive. Octahedral rotations are small and present only in Ca proximity. This is consistent with what were observed for other compositions.^[43–45] Ca and Zr disorder is not included in our model. By observing that in the NWs the unit cell volume decreased, we conjecture that the tetragonal off-centerings were quenched at lower temperature, this resulted

in an extended stability of the rhombohedral phase. As temperature increased and volume expanded the tetragonal distortions became more favored but due to the preferential orientation of the crystallites the tetragonal phase manifested only at higher temperature as compared to the bulk. Our conjecture was validated by comparing predicted structures with experimental XRD data, as shown in Figure 5c (Section S8 and Figure S10, Supporting Information). From the point of view of symmetry, the lowest energy structures compatible with the experimental lattice parameter at $T = 30, 230,$ and 430 °C exhibited rhombohedral (space group no. 160), monoclinic (space group no. 8), and rhombohedral (again space group no. 160) symmetry, respectively. The appearance of an average monoclinic phase might be the origin of the piezoelectric behavior similar to what is observed in PZT, although the coupling in our case is lower than PZT.^[46]

Similar enhancement of spontaneous polarization was theoretically predicted due to the nanosize confinement in PbTiO₃ NWs.^[4] Negative-pressure-driven enhancement of the tetragonality, Curie temperature, and spontaneous polarization in

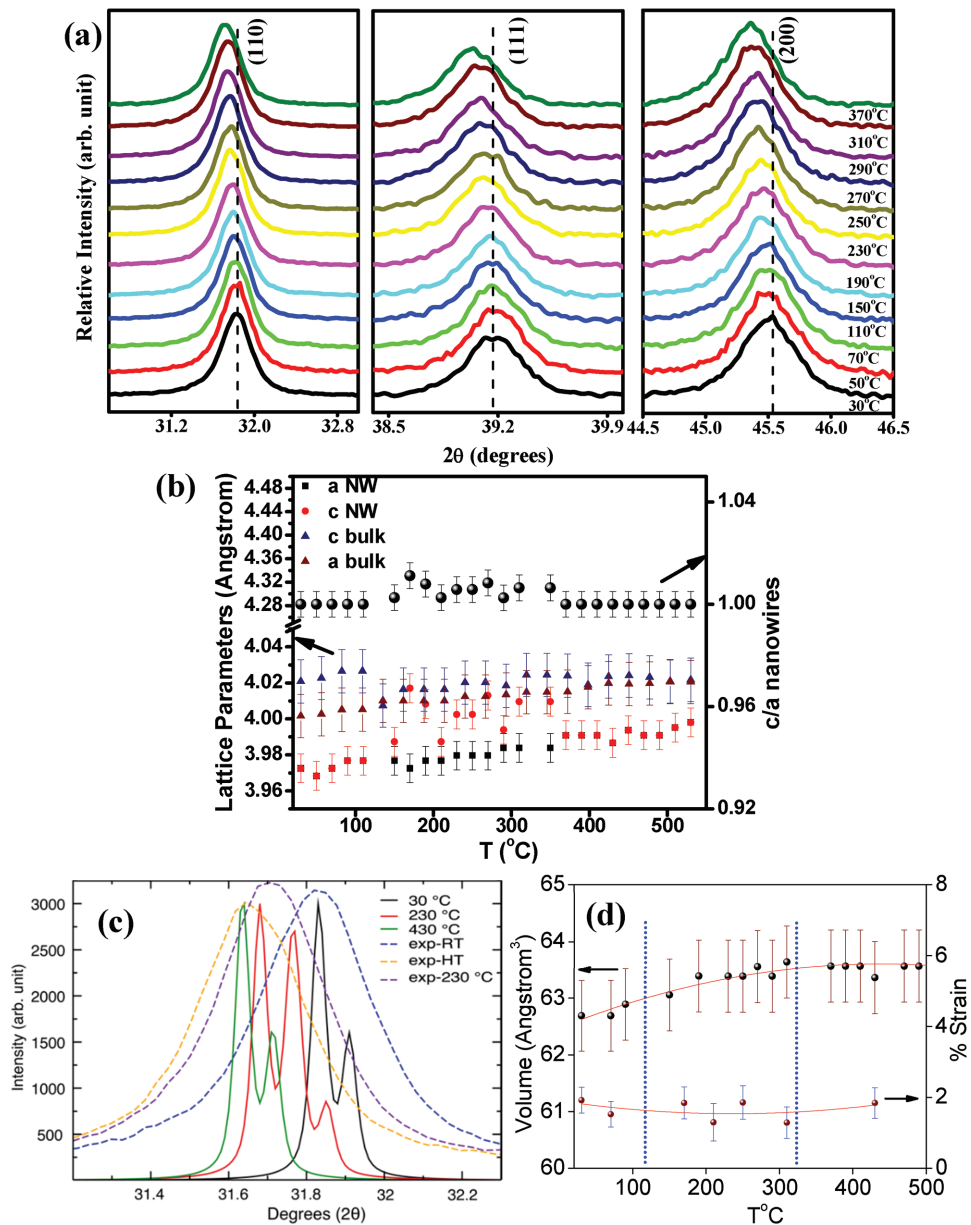


Figure 5. Strain induced by lattice contraction in BCT-0.5BZT nanowires. a) XRD patterns of BCT-0.5BZT nanowires showing shift in the peak positions toward low angle 2θ with increasing temperature (temperatures marked). b) a , c , and c/a ratios of bulk and BCT-0.5BZT nanowires showing enhanced tetragonality between 100 and 300 °C. Error bars in estimation of the lattice parameters are also shown. c) Comparison between experimental and theoretically computed XRD spectra (near $2\theta = 31.8^\circ$). d) Change in the unit-cell volume and % strain BCT-0.5BZT nanowires as a function of temperature as calculated from the shift in the XRD peak positions as shown in (a).

freestanding PbTiO_3 NWs was also reported, driven by stress that developed during transformation of the material from a lower-density crystal structure to the perovskite phase,^[3,17] however this did not seem to be the case for BZT-0.5BCT NWs. Apart from lead-based ferroelectrics, a few recent studies have been focused on discovering stress-induced enhancement of ferroelectric properties in Pb-free perovskite system, essentially in BaTiO_3 and its alloys.^[2,14,15,47] It is clearly understood that the ferroelectric phase transition enhancements cannot be related to a purely size effect, which can appear only for a shorter length scale.^[24,48,49] The strained unit-cell relative to

the bulk BCT-0.5BZT is indicated, (Figure 5d) where more of a 1.5% stress (Figure 5d) was calculated by Williamson–Hall plot (Section S9 and Figure S11, Supporting Information). While the amount of the strain may be lower in the BCT-0.5BZT bulk due to free-formed grains and hence unstrained ferroelectric domains, the stress caused by 1D confinement and increased grain boundaries in the oriented crystallites in BCT-0.5BZT NWs lead to the enhancement in the spontaneous polarization and subsequent shift in T_C . As it is difficult to interpret structural data from systems with small crystallite size as in our case, the direct evidence of phase transitions from electrical

measurements as well as our first principle calculations considered in combination gives a reliable interpretation.

3. Conclusions

In summary, for the first time, phase-stabilized BCT-0.5BZT polycrystalline NWs with high aspect ratio were prepared using a simple, scalable sol-gel assisted template-wetting methodology. BCT-0.5BZT NWs exhibit a largely increased T_C of ≈ 300 °C as compared to ≈ 95 °C in bulk of similar composition. The NWs showed a measurable ferroelectric polarization of $P_r \approx 3$ $\mu\text{C cm}^{-2}$ and piezoelectric d_{33} coupling coefficient ≈ 35 pmV^{-1} at room temperature indicating the suitability of BCT-0.5BZT NWs as a promising Pb-free ferroelectric/piezoceramic alternative. The origin of the enhanced T_C was supported by theoretical modeling that aided the interpretation of the experimental data. We observed volume expansion around the $T_C \approx 300$ °C, possibly due to the strain relaxation and phase change phenomena. Overall, the BCT-BZT NWs exhibited contracted lattice volume with respect to the bulk and were hence strained even at room temperature, which explains the observed phase transition shift to a large extent. Our new synthesis technique has shown that is possible to improve the temperature dependence of ferroelectric properties in Pb-free NWs by controlling morphology and strain at the nanoscale.

4. Experimental Section

BCT-0.5BZT Sol Preparation: BCT-0.5BZT sol was prepared using barium acetate, calcium acetate, titanium (IV) isopropoxide, and zirconyl oxychloride octahydrate. First, stoichiometric amounts of titanium isopropoxide and zirconyl oxychloride (as for $(\text{Ba}_{0.85}\text{Ca}_{0.15})(\text{Zr}_{0.1}\text{Ti}_{0.9}\text{O}_3)$) in the stoichiometric ratio were dissolved in a mixture of absolute ethanol and glacial acetic acid. An amount of acetyl acetone was added as a chelating agent in a molar ratio 1:1 with respect to titanium. Separately, barium and calcium acetates in stoichiometric amounts were dissolved in warm acetic acid (60 °C). The titanium and zirconium solution were then added dropwise to the calcium and barium solution under vigorous stirring at room temperature. Finally, deionized water (1:50 molar ratio with respect to titanium) was added to initiate the hydrolysis process and lactic acid for adjusting the pH at a value of about 3.5. The amount of solvent was adjusted so that the concentration of titanium in the final sol is about 0.3–0.4 M. The resultant clear yellowish sol was then left stirring overnight. All the chemicals were of ACS grade and were obtained from Sigma-Aldrich with minimum 99.99% purity. The chemicals were used as-received.

Sol Infiltration in PI Template and BCT-0.5BZT Crystallization: The PI porous templates from ipPore (it4ip) of 20 μm thickness and a 200 nm average pore diameter with a well-defined minimum pore density of 1E^3 were used for infiltration of BCT-0.5BZT sol. The templates were cleaned prior to infiltration successively in isopropanol, deionized water, and acetone. After cleaning, the templates were placed onto a filter paper (GE health sciences) in a filtration set-up. The sol prepared above was then drop-casted onto the template and vacuum infiltrated within the pores. The sol containing the Ba, Ca, Ti, and Zr precursors was allowed to infiltrate and polymerize within the pores of polyimide membrane pores after which they were then placed on a silicon substrate and air dried at 60 °C in a drying oven for 12 h followed by air annealing at 1000 °C for 24 h. After the decomposition of the polyimide membrane, white powdery film of BCT-0.5BZT NWs was obtained on the Si substrate. The remaining sol was heated at 60 °C until a gel formed and then dried

at 120 °C overnight on a hot plate. The dried powder was calcined at 1000 °C and was also characterized to understand the crystallization of BCT-0.5BZT.

Characterization: The phase and crystallinity of the BCT-0.5BZT NWs were characterized by XRD with a Bruker D8 diffractometer equipped with Lynx Eye position-sensitive detector using Cu $K\alpha$ radiation ($\lambda = 1.5418$ Å) at room temperature. High temperature XRD measurements were carried out by a D8 ADVANCE Bruker diffractometer equipped with Goebel Mirror for parallel beam with a VANTEC-1 fast detector and an MIR heating stage allowing in situ XRD collections up to 500 °C at 20 °C intervals and a resolution of 0.001°. In all cases, peak shifts due to sample misalignment were adjusted while performing the XRD scans and background correction was taken care by using a zero diffraction silicon substrate for mounting. Microstructural studies were carried out by field-emission SEM (FEI Nova NanoSEM) and HRTEM (JEOL 4000EXII). Calorimetric curves of the dried powder were recorded in nitrogen (100 cm^3 min^{-1}) on a simultaneous TG/DSC instrument (Q600 SDT, TA Instruments) in closed aluminum pans at a heating rate of 10 °C min^{-1} . FTIR measurements were carried out using a Bruker Tensor 27 IR spectrometer with attenuated total internal reflection attachment. Following a baseline measurement, the samples were placed on an IR transparent high refractive index crystal on which the IR beam was incident and pressure was applied from a small metal disk to ensure contact between the sample and the crystal. IR spectrograms were generated with an average of 20 spectra taken for each measurement.

Dielectric Permittivity, Ferroelectricity, and Piezoelectric Response: For dielectric permittivity versus temperature measurements and ferroelectric polarization versus electric field (P - E loops), BCT-0.5BZT NW network films of ≈ 5 μm thickness on Au/Si were prepared by mixing the NWs with a little quantity of dimethylformamide, which was then dried at ≈ 200 °C to improve the adhesion of the network film to the substrate. Top electrodes of ≈ 100 μm were then deposited using conductive silver epoxy and attaching copper wires. The measurement was carried out in an inert sealed bespoke chamber with a heating and cooling rate of 2 °C min^{-1} (using 336 Temperature Controller, Lakeshore), while the dielectric properties were recorded between frequencies of 1 kHz and 2 MHz using an impedance analyzer (4294A, Agilent Technologies).

To measure the ferroelectric hysteresis loops, top Au electrodes were deposited on the BCT-0.5BZT NW network film using a CRC-100 sputtering system (Plasma Sciences Inc.) and through a shadow mask that produced 50 μm diameter dots for a thickness of 100 nm. The polarization measurements of the fabricated nanostructured (using Au top-bottom electrodes) capacitors were performed at different temperatures using a commercial Radiant Precision LC Ferroelectric tester (from Radiant Technologies, Inc.) equipped with a microprobe station. The heating was carried out using a custom-made heater set-up to measure polarizations at different temperatures. The polarization data were collected independently from several (more than 20) top electrodes keeping the same bottom electrode and were found to be consistent. During the hysteresis measurements, a constant standard bipolar input profile was used at 100 ms period.

The piezoelectric coefficient of the BCT-0.5BZT NW network was measured with a PFM setup, using a Bruker Multimode 8 microscope, and a Nanoscope 5 controller. BCT-0.5BZT NW network film was cast on a gold-coated ITO using the similar process used for the dielectric measurement. For PFM the sample was mounted on a standard conductive AFM holder disk, held and contacted by Ag-paint. The voltages were applied to the sample, while the tip was grounded. The AC frequency used was 150 kHz. A calibration procedure was performed on Bruker's PFM-SMPL LiNbO_3 calibration sample in order to extract effective piezoelectric coefficients from the measurements. The deflection sensitivity at the operation conditions was calculated from the corrected AC deflection of the calibration sample, using the value of $d_{33} = 7.5$ pmV^{-1} , specified by calibration sample supplier (Figure S8, Supporting Information).

Theoretical Calculations: First-principles calculations were performed with the Quantum Espresso package,^[50] using ultrasoft PBEsol

pseudopotentials.^[51] Ba₇CaTi₇ZrO₂₄ was used to model the experimental composition. The kinetic energy cutoff and the charge density cutoff were set to be 40 and 480 Ry, respectively. A 3 × 3 × 3 mesh was used to sample the Brillouin zone. During the geometry optimizations a convergence threshold of 0.02 eV Å⁻¹ was used for the residual forces and 0.1 kbar for the pressure. The fully relaxed ground state for the supercell was tetragonal with *a* = 4.0 Å and *c/a* = 1.015. The cell symmetry was analyzed with FINDSYM.^[52]

Supporting Information

Supporting Information is available from the Wiley Online Library or from the author.

Acknowledgements

This work was financially supported by the European Research Council through an ERC Starting Grant (Grant No. ERC-2014-STG-639526, NANOGEN). S.K.-N., A.D. and Y.C. are grateful for financial support from this same grant. S.-L.S. acknowledges funding through the EPSRC grant EP/M010589/1. C.O. acknowledges studentship funding from the China Scholarship Council and the Cambridge Commonwealth, European and International Trust. M.F. acknowledges collaboration with the AFLOW Consortium (<http://www.aflow.org>) under the sponsorship of DOD-ONR (N000141310635 and N000141512266). P.E.S.-J. was supported by a Marie Curie–Junta de Andalucía Postdoc Talentia grant. Supporting data for this paper is available at the DSpace@Cambridge data repository (<https://dx.doi.org/10.17863/CAM.9457>).

Conflict of Interest

The authors declare no conflict of interest.

Keywords

Curie temperature, ferroelectric materials, lead-free oxides, nanowires, sol–gel synthesis, template wetting

Received: March 2, 2017

Revised: April 12, 2017

Published online: June 1, 2017

- [1] J. F. Scott, A. C. A. de Paz, *Science* **1989**, 246, 1400.
- [2] S. A. Harrington, J. Zhai, S. Denev, V. Gopalan, H. Wang, Z. Bi, S. A. T. Redfern, S.-H. Baek, C. W. Bark, C.-B. Eom, Q. Jia, M. E. Vickers, J. L. MacManus-Driscoll, *Nat. Nanotechnol.* **2011**, 6, 491.
- [3] J. Wang, B. Wylie-van Eerd, T. Sluka, C. Sandu, M. Cantoni, X. K. Wei, A. Kvasov, L. J. McGilly, P. Gemeiner, B. Dkhil, A. Tagantsev, J. Trodahl, N. Setter, *Nat. Mater.* **2015**, 4, 985.
- [4] M. Q. Cai, Y. Zheng, B. Wang, G. W. Yang, *Appl. Phys. Lett.* **2009**, 95, 232901.
- [5] J. E. Spanier, A. M. Kolpak, J. J. Urban, I. Grinberg, L. Ouyang, W. S. Yun, A. M. Rappe, H. Park, *Nano Lett.* **2006**, 6, 735.
- [6] A. F. Devonshire, *Philos. Mag.* **1951**, 42, 1065.
- [7] N. A. Pertsev, A. G. Zembilgotov, A. K. Tagantsev, *Phys. Rev. Lett.* **1998**, 80, 1988.
- [8] Y. L. Li, S. Y. Hu, Z. K. Liu, L. Q. Chen, *Appl. Phys. Lett.* **2001**, 78, 3878.

- [9] M. Sepliarsky, S. R. Phillpot, M. G. Stachiotti, R. L. Migoni, *J. Appl. Phys.* **2002**, 91, 3165.
- [10] J. B. Neaton, K. M. Rabe, *Appl. Phys. Lett.* **2003**, 82, 1586.
- [11] E. D. Specht, H.-M. Christen, D. P. Norton, L. A. Boatner, *Phys. Rev. Lett.* **1998**, 80, 4317.
- [12] N. Yanase, K. Abe, N. Fukushima, T. Kawakubo, *Jpn. J. Appl. Phys.* **1999**, 38, 5305.
- [13] S. K. Streiffer, J. A. Eastman, D. D. Fong, C. Thompson, A. Munkholm, M. V. Ramana, O. Auciello, G. R. Bai, G. B. Stephenson, *Phys. Rev. Lett.* **2002**, 89, 067601.
- [14] K. J. Choi, M. Biegalski, Y. L. Li, A. Sharan, J. Schubert, R. Uecker, P. Reiche, Y. B. Chen, X. Q. Pan, V. Gopalan, L. Q. Chen, D. G. Schlom, C. B. Eom, *Science* **2004**, 306, 1005.
- [15] W. L. Li, T. D. Zhang, Y. F. Hou, Y. Zhao, D. Xu, W. P. Cao, W. D. Fei, *RSC Adv.* **2014**, 4, 56933.
- [16] A. R. Damodaran, E. Breckenfeld, Z. Chen, S. Lee, L. W. Martin, *Adv. Mater.* **2014**, 26, 6341.
- [17] A. Kvasov, L. J. McGilly, J. Wang, Z. Shi, C. S. Sandu, T. Sluka, A. K. Tagantsev, N. Setter, *Nat. Commun.* **2015**, 7, 12136.
- [18] B. Fu, Y. Yang, K. Gao, Y. Wang, *Appl. Phys. Lett.* **2015**, 107, 042903.
- [19] W. Liu, X. Ren, *Phys. Rev. Lett.* **2009**, 103, 257602.
- [20] J. Wu, D. Xiao, J. Zhu, *Chem. Rev.* **2015**, 115, 2559.
- [21] D. E. Cox, B. Noheda, G. Shirane, Y. Uesu, K. Fujishiro, Y. Yamada, *Appl. Phys. Lett.* **2001**, 79, 400.
- [22] M. Acosta, N. Novak, W. Jo, J. Rödel, *Acta Mater.* **2014**, 80, 48.
- [23] J. P. B. Silva, E. C. Queiros, P. B. Tavares, K. C. Sekhar, K. Kamakshi, J. Agostinho Moreira, A. Almeida, M. Pereira, M. J. M. Gomes, *J. Electroceram.* **2015**, 35, 135.
- [24] D. R. Brandt, J. M. Acosta, J. Koruza, K. G. Webbe, *J. Appl. Phys.* **2014**, 115, 204107.
- [25] R. E. Cohen, *Nature* **1992**, 358, 136.
- [26] Z. Zhou, C. C. Bowland, M. H. Malakooti, H. Tang, H. A. Sodano, *Nanoscale* **2016**, 8, 5098.
- [27] W. Wu, L. Cheng, S. Bai, W. Dou, Q. Xu, Z. Wei, Y. Qin, *J. Mater. Chem. A* **2013**, 1, 7332.
- [28] D.-J. Liaw, K.-L. Wang, Y.-C. Huang, K.-R. Lee, J.-Y. Lai, C.-S. Ha, *Prog. Polym. Sci.* **2012**, 37, 907.
- [29] P. Bharathi, P. Thomas, K. B. R. Varma, *J. Mater. Chem. C* **2015**, 3, 4762.
- [30] A. Datta, D. Mukherjee, C. Kons, S. Witanachchi, P. Mukherjee, *Small* **2014**, 10, 4093.
- [31] A. Datta, D. Mukherjee, S. Witanachchi, P. Mukherjee, *Adv. Funct. Mater.* **2014**, 24, 2638.
- [32] D. Mukherjee, A. Datta, C. Kons, M. Hordagoda, S. Witanachchi, P. Mukherjee, *Appl. Phys. Lett.* **2014**, 105, 212903.
- [33] J. Varghese, S. Barth, L. Keeney, R. W. Whatmore, J. D. Holmes, *Nano Lett.* **2012**, 12, 868.
- [34] J. Kim, S. A. Yang, Y. C. Choi, J. K. Han, K. O. Jeong, Y. J. Yun, D. J. Kim, S. M. Yang, D. Yoon, H. Cheong, K. S. Chang, T. W. Noh, S. D. Bu, *Nano Lett.* **2008**, 8, 1813.
- [35] R. A. Whiter, Y. Calahorra, C. Ou, S. Kar-Narayan, *Macromol. Mater. Eng.* **2016**, 301, 1016.
- [36] Y. C. Yang, C. Song, X. H. Wang, F. Zeng, F. Pan, *Appl. Phys. Lett.* **2008**, 92, 012907.
- [37] M. Kuwabara, K. Goda, K. Oshima, *Phys. Rev. B* **1990**, 42, 10012.
- [38] G. Chen, X. Wang, J. Lin, W. Yang, H. Li, Y. Wen, L. Li, Z. Jiang, Q. Lei, *J. Mater. Chem. C* **2016**, 4, 8070.
- [39] B. Jaffe, W. Cook, H. Jaffe, *Non-Metallic Solids, Piezoelectric Ceramics*, Vol. 3, (Eds: J. P. Roberts, P. Popper), Academic Press, London **1971**, p. 317.
- [40] Q. G. Chi, J. F. Dong, C. H. Zhang, C. P. Wong, X. Wang, Q. Q. Lei, *J. Mater. Chem. C* **2016**, 4, 8179.

- [41] M. Fornari, D. J. Singh, *Phys. Rev. B* **2001**, *63*, 92101.
- [42] J. M. Rondinelli, C. J. Fennie, *Adv. Mater.* **2012**, *24*, 1961.
- [43] M. Ghita, M. Fornari, S. V. Halilov, D. J. Singh, *Phys. Rev. B* **2005**, *72*, 054114.
- [44] R. Armiento, B. Kozinsky, M. Fornari, G. Ceder, *Phys. Rev. B* **2011**, *84*, 014103.
- [45] R. Armiento, B. Kozinsky, G. Hautier, M. Fornari, G. Ceder, *Phys. Rev. B* **2014**, *89*, 134103.
- [46] B. Noheda, D. E. Cox, G. Shirane, J. A. Gonzalo, L. E. Cross, S.-E. Park, *Appl. Phys. Lett.* **1999**, *74*, 2059.
- [47] M. C. Ehmke, S. N. Ehrlich, J. E. Blendell, K. J. Bowman, *J. Appl. Phys.* **2012**, *111*, 1241101.
- [48] J. Junquera, P. Ghosez, *Nature* **2003**, *422*, 506.
- [49] J. E. Spanier, A. M. Kolpak, J. J. Urban, I. Grinberg, L. Ouyang, W. S. Yun, A. M. Rappe, H. Park, *Nano Lett.* **2006**, *6*, 735.
- [50] P. Giannozzi, S. Baroni, N. Bonini, M. Calandra, R. Car, C. Cavazzoni, D. Ceresoli, G. L. Chiarotti, M. Cococcioni, I. Dabo, A. D. Corso, S. de Gironcoli, S. Fabris, G. Fratesi, R. Gebauer, U. Gertsmann, C. Gougousis, A. Kokalj, M. Lazzeri, L. Martin-Samos, N. Marzari, F. Mauri, R. Mazzarello, S. Paolini, A. Pasquarello, A. L. Paulatto, C. Sbraccia, S. Scandolo, G. Sclauzero, A. P. Seitsonen, A. Smogunov, P. Umari, R. M. Wentzcovitch, *J. Phys.: Condens. Matter* **2009**, *21*, 395502.
- [51] K. F. Garrity, J. W. Bennett, K. M. Rabe, D. Vanderbilt, *Comput. Mater. Sci.* **2014**, *81*, 446.
- [52] H. T. Stokes, D. M. Hatch, *J. Appl. Cryst.* **2005**, *38*, 237.